MPS	Journal	MSP No.	Dispatch: April 14, 2023	CE:
	MACO	202213689	No. of Pages: 9	PE: Praveendra Kumar

Received: 6 December 2022 | Accepted: 20 March 2023

DOI: 10.1002/maco.202213689

ARTICLE

Materials and Corrosion

Monitoring the galvanic corrosion of copper–steel coupling in bentonite slurry during the early oxic phase using coupled multielectrode arrays

Tadeja Kosec | Miha Hren | Klara Prijatelj | Bojan Zajec | Nina Gartner | Andraž Legat

Slovenian National Building and Civil Engineering Institute, Ljubljana, Slovenia

Correspondence
Tadeja Kosec, Slovenian National Building and Civil Engineering Institute, Dimičeva 12, Ljubljana 1000, Slovenia.
Email: tadeja.kosec@zag.si

Funding information
Javna Agencija za Raziskovalno Dejavnost RS

Abstract

In the case of a two-part container for spent nuclear fuel, consisting of an iron-based inner structure with a copper coating, the potential perforation of copper through minor damage may result in intensive galvanic corrosion between copper and steel. The present work focuses on the corrosion of steel galvanically coupled to copper and exposed to a slightly saline environment under oxic conditions. The electrochemical processes on individual electrodes were monitored by coupled multielectrode arrays (CMEAs). The CMEAs were either in contact with groundwater saturated with bentonite or immersed in groundwater only. Very high galvanic corrosion currents were detected between carbon steel and pure copper in the early oxic phase. Additionally, the use of CMEAs further made it possible to monitor the distribution of cathodic currents around the steel electrode, which behaved anodically. Various microscopy and spectroscopy techniques were applied to identify the modes of corrosion and the type of corrosion products present at the end of the period of exposure.

KEYWORDS

Aspö groundwater, bentonite, copper, coupled multielectrode array, electrochemical properties, Raman analysis, steel

1 | INTRODUCTION

Since copper is the only absolute barrier preventing the release of radionuclides in the case of Swedish/Finnish, Canadian, and other world's high-level radioactive waste disposal programs (including Taiwan, Korea, Japan, and Switzerland), the corrosion of copper has been studied extensively in various environments and conditions simulating various times after emplacement.[1–11]

The lifespan of the Cu container is designed to be above 10^6 years.[2] Upon sealing, a limited amount of air becomes trapped in the repository, in the low-permeability groundwater-saturated bentonite surrounding the container.[1] This O_2 is then consumed by various reactions and also by corrosion of the copper container. The time for the predicted O_2 concentration to decrease to 1% of the initial level ranged between 10 and 300 years in deep geological repository (DGR) in granite rock[2] and 40 and additional 30 years in the case of DGR in opalinus clay.[3] The elapsed time at which the transition to anoxic conditions occurred was estimated to be within the same time range.[2] Once this O_2 has been fully consumed, it is most likely that further corrosion is sustained through the supply of dissolved SH^- to the copper surface.[1] Cu

corrosion in sulfide systems under anoxic conditions has therefore been studied extensively.[6–9]

Lately, many studies have been devoted to understanding the effect of varying anion concentrations on the adsorption of HS^- on copper under anoxic conditions.[8,9] It is, however, likely, that small amounts of sulfide could also influence corrosion during the early oxic repository period.

In the Canadian approach, the design of the container for the permanent disposal of spent nuclear fuel in a deep geological repository involves a carbon steel (CS) vessel coated with a 3 mm layer of copper. In the event of an undetected defect in the Cu coating, the underlying CS could be exposed to the groundwater, potentially accelerating the galvanical corrosion of CS.[10–13]

Recent studies have simulated a defect in a cold-sprayed coating and reported that corrosion proceeds via the galvanic coupling and oxygen reduction at the surface.[10,11] Besides the accumulation of damage at the base of the defect, corrosion propagated along the copper/steel interface, most likely resulting from damage inflicted during the deposition process.[10,11]

One study investigated the influence of the Cu:CS area ratio and anion concentrations on corrosion by monitoring the galvanic current and galvanic potential at Cu:CS area ratios of 1:1 to 2500:1 and $[Cl^-]$ concentrations between 0.001 and 3.0 M.[12] It was found that, in the presence of oxygen, the galvanic coupling with Cu enhances the corrosion rate of CS, since the reduction of O_2 on Cu is the driving force behind the accelerated galvanic corrosion of CS. Furthermore, a larger current is generated when the Cu:CS area ratio is as large as 1000.[12,13]

Our study using Cu electrical resistance sensors corrosion under oxic conditions in bentonite with Aspö groundwater resulted in a corrosion rate of around 1 $\mu m\ year^{-1}$ monitored through 3.5 years of exposure.[14,15] There, the reduction of thickness and impedance measurements were used to evaluate the corrosion rate on copper electrical resistance sensors. The effects of the solution chemistry in the presence of bentonite in oxic conditions proved two different modes of corrosion, dependent on whether the copper was in the solution or the bentonite slurry.[16] A coupled multielectrode array (CMEA) was also used to monitor the spatio-temporal distribution of currents in bentonite slurry, where the consumption of O_2 was reflected by the detection of smaller currents.[17] The use of multielectrode arrays using a multichannel microelectrode analyzer has also been demonstrated for copper pitting probability studies in chloride media.[18]

From the current state-of-the-art review presented here, and the majority of recent research,[19,20] it is clear that several issues remain unanswered.

The purpose of this research was to characterize the corrosion behavior of copper and steel in an aqueous solution and in a bentonite environment saturated with saline groundwater at open circuit potential and room temperature. Considerable attention was given to the spatio-temporal evolution and intensity of the anodic activities on the steel electrode and the cathodic activities on the copper electrodes in the early days of exposure to oxic environments. CMEAs were implemented for this purpose and partial anodic and cathodic currents were monitored at high sampling rates over a 2-week period. Microscopic and spectroscopic investigation of surface modifications was carried out following a period of exposure to saline groundwater and bentonite. MicroCT scans of the electrodes were also conducted to verify the type and volume of the corroded damage.

2 | MATERIALS AND METHODS

2.1 | CMEAs

The CMEA was constructed using 24 copper electrodes and 1 steel wire electrode, each with a diameter of 0.50 mm. The chemical composition of CS wire was verified by optical emission spectroscopy SpectroMAXx (Spectro Ametek), while 99.99 wt.% insulated Cu wire was purchased from Goodfellow. The electrodes were arranged in a 5×5 array, with the steel electrode positioned in the middle, then embedded in epoxy resin (Figure 1b). The nominal surface area of one electrode was 0.00196 cm^2, and the center-to-center distance between electrodes was approximately 1 mm. Before conducting measurements, the specimens were abraded with 2400-grid emery paper, then ultrasonically degreased in ethanol for 3 min and thoroughly dried.

CMEA aims to separate an investigated piece of metal (in our case a steel-copper pair) into smaller sections to enable the measurement of coupling currents between these sections (electrodes). Each coupling current is measured by ZRA, hence all sections are at the same electrical potential. The current measurement is passive, since no potentials or current are being impressed. Actually, CMEA is mimicking the entire electrode area, and consequently spatiotemporal corrosion pattern (distribution of anodic and cathodic currents over time) can be monitored.[21,22]

Throughout the exposure, all 25 electrodes were electrically coupled through a system of zero-resistance ammeters (Figure 1a). The cathodic and anodic corrosion currents were continuously monitored at a frequency of 1 Hz. The specimen was exposed to two different conditions: saline groundwater with bentonite and saline

COLOR FIG

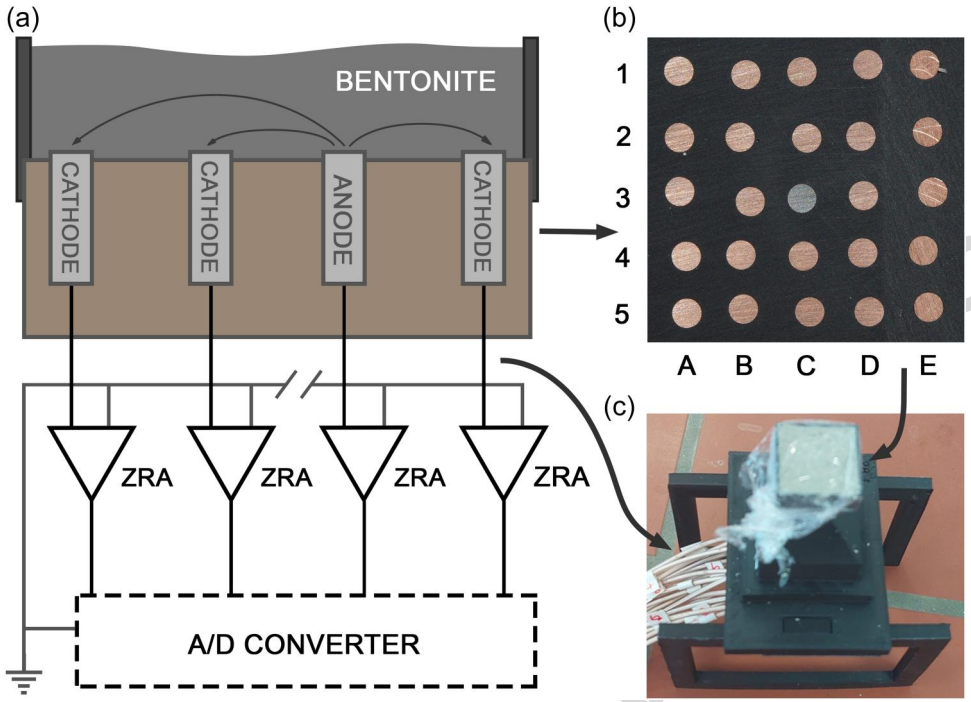

FIGURE 1 (a) Schematic representation of the ZRA system, (b) top view of the coupled multielectrode arrays (CMEAs) specimen before exposure, and (c) side view of the CMEA specimen during exposure to bentonite.

groundwater only. The two types of exposure were monitored separately, with the specimen abraded and degreased before each exposure. Exposure to these conditions continued until the corrosion currents reached very low cathodic and anodic activity, which occurred at 13 days in the bentonite and 6 days in the groundwater.

The chemical composition of the Aspö groundwater was 0.181 M Cl^-, 0.44 mM HCO_3^-, 4.6 mM SO_4^{2-} and 0.005 mM HS^-. Analytical-grade sodium compounds were used for preparation of the solution. The pH of the solution was 7.2.

Bentonite slurry was prepared by combining 25 g of bentonite and 100 mL of groundwater. The Wyoming bentonite, MX-80 with ~75% sodium montmorillonite with sheet-like crystal structure was used.[12] A 15 mm thick layer of bentonite slurry was poured over the CMEA electrodes, forming a 30 × 30 × 20 mm pond, then it was covered with a parafilm to avoid it drying out.

2.2 | Electrochemical measurements

A three-electrode corrosion cell with a volume of 350 cm^3 was used with a working electrode area of 0.785 cm^2. A Gamry 600 potentiostat/galvanostat was used for electrochemical tests. All potentials are reported with respect to the Ag/AgCl scale.

The electrochemical tests consisted of a stabilization time at open circuit potential (OCP) for a minimum of 2 h, followed by linear polarization measurements at a scan rate of 0.1 mV s^{-1} ± 20 mV versus OCP and potentiodynamic scans at a scan rate of 0.16 mV s^{-1}.

2.3 | Surface characterization and spectroscopic analysis

The surface morphology of the CMEA electrodes was inspected and analyzed using a scanning electron microscope (SEM, JSM-IT5500LV, JEOL, Japan), at an acceleration voltage of 20 kV. The elementary compositions of the corrosion products formed on the metal surface were investigated by means of an energy dispersive X-ray spectroscopy (EDS, Oxford Instruments) analyzer.

An Xradia microXCT-400 (Xradia, 2011, USA) tomography device was used to characterize the type and extent of corrosion damage. The scans were conducted at 150 kV using two different lenses, obtaining resolutions of 8.17 and 1.03 μm for the lower and higher magnifications, respectively.

Horiba Jobin Yvon LabRAM HR800 Raman spectrometer coupled to an Olympus BXFM optical microscope was used for obtaining Raman spectra using a 633 nm laser excitation line, a 100× objective lens and a

COLOR FIG

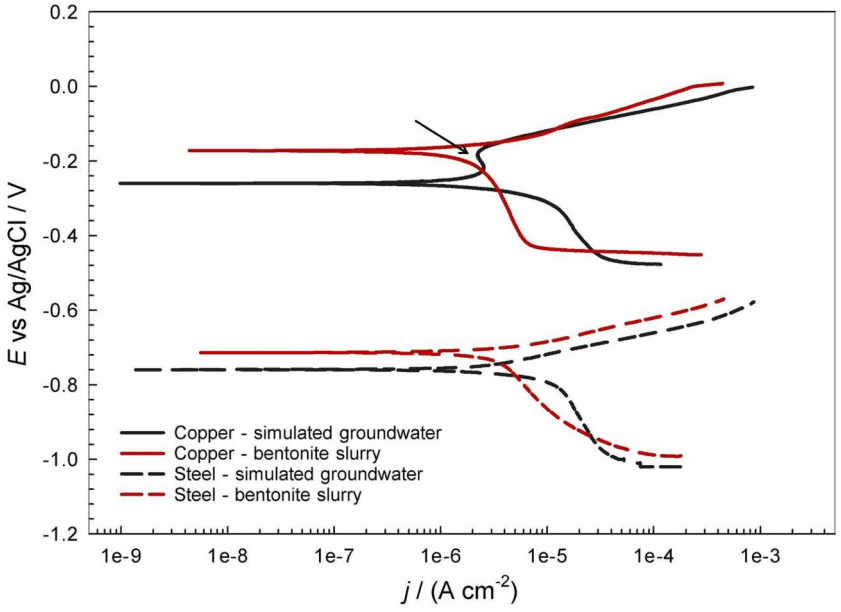

FIGURE 2 Potentiodynamic curves at 0.166 mV s^{-1} for copper and steel electrodes in simulated groundwater and bentonite slurry.

600 grooves/mm grating, which gave a spectral resolution of 2 cm^{-1}/pixel. A multichannel air-cooled CCD detector was used. The spectra presented are without baseline correction.

3 | RESULTS

3.1 | Electrochemical measurements

To study the electrochemical behavior of copper and steel in saline groundwater under oxic conditions, potentiodynamic scans were obtained in a groundwater solution and in a bentonite slurry on each individual electrode (Figure 2). For copper, the cathodic part of the potentiodynamic scan showed lower current densities in the bentonite slurry, when compared to cathodic current densities of Cu in simulated groundwater. It is assumed that this is due to the reduced amount of oxygen in the near vicinity of the electrode. In the anodic part of the potentiodynamic scan for Cu, active-to-passive transition was observed in simulated groundwater (see arrow in Figure 2), most probably due to Cu_2S inhibiting anodic dissolution, even at such small concentrations. This process has been described previously.[15] Such active-to-passive transition was not observed in the bentonite slurry (Figure 2). For the steel electrode, active dissolution was observed in both the simulated groundwater and the bentonite slurry, with the corrosion current densities being slightly higher than those observed for copper (see values in Table 1). In steel, a smaller current density was also observed in the cathodic region in the bentonite slurry. In the case of both steel and copper, the corrosion potential, E_{corr}, moved to higher potentials in the bentonite slurry.

TABLE 1 Electrochemical parameters deduced from potentiodynamic curves.

		E_{corr}/V	j_{corr}/A cm^{-2}
Simulated groundwater	Copper	−0.260	$0.894 \cdot 10^{-6}$
	Steel	−0.760	$1.43 \cdot 10^{-6}$
Bentonite Slurry	Copper	−0.172	$0.585 \cdot 10^{-6}$
	Steel	−0.714	$1.20 \cdot 10^{-6}$

3.2 | CMEA measurements in bentonite slurry

Results of the 13-day period of exposure to bentonite slurry are presented in Figure 3a. Immediately after pouring the slurry into the basin over the CMEA electrodes, the anodic peak emerging from the CS electrode (C3) increased to over 1200 μA cm^{-2}. After this, the current then steadily decreased for the duration of the 14-day exposure. The mixture of corrosion products with the surrounding bentonite saturated the exposed surface of the steel, causing the anodic current to decrease. The remaining 24 copper electrodes behaved cathodically, with the electrodes closer to the steel being less net cathodic than the electrodes further away, as can be seen from the average current densities (Figure 3b). Using the CMEA technique, the total volume of damage was calculated to be 9.3×10^6 μm^3, which resulted in approximately 47 μm of corrosion damage on the steel

COLOR FIG

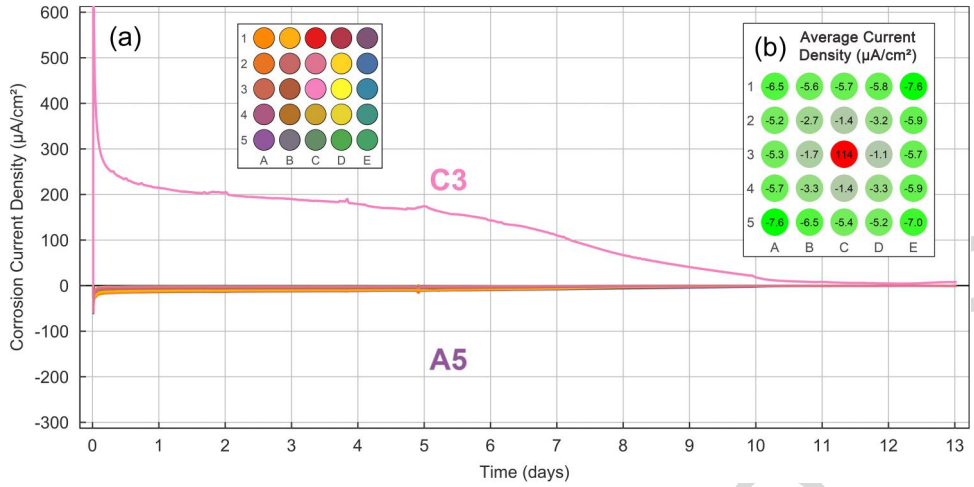

FIGURE 3 (a) Evolution of current in copper-steel coupled multielectrode array (CMEA) electrodes over 13 days of exposure to bentonite slurry soaked with simulated Aspö groundwater, and (b) average corrosion current densities (in μA cm^{-2}) for the individual CMEA electrodes. Cathodic currents are represented in green and anodic currents in red.

COLOR FIG

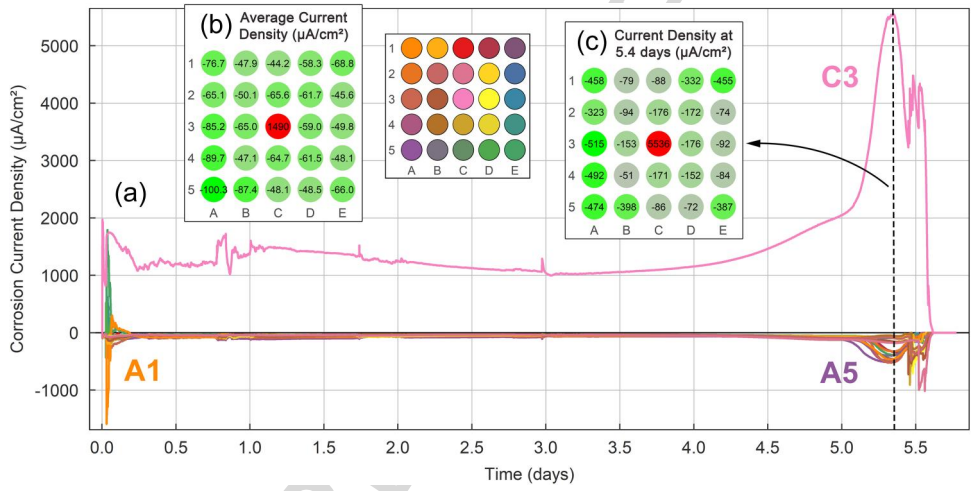

FIGURE 4 (a) Evolution of current in copper-steel coupled multielectrode array (CMEA) electrodes over 6 days of exposure to simulated Aspö groundwater, (b) average corrosion current densities (in μA cm^{-2}) for the individual CMEA electrodes, and (c) corrosion current densities at Day 5.4 (in μA cm^{-2}). The cathodic currents are shown in green and the anodic currents in red.

electrode. This further translated to an average corrosion rate of approximately 1.3 mm $year^{-1}$ during the first 13 days of exposure.

3.3 | CMEA measurements in Aspö groundwater

Compared to the measurements in bentonite slurry, more intensive galvanic corrosion was observed in simulated Aspö groundwater. Figure 4a shows the corrosion current density over time for each electrode exposed to the simulated Aspö groundwater. Some cathodic and anodic activity was initially observed on multiple electrodes (A5, D5, and E5), but anodic activity was only maintained on the steel C3 electrode, where it fluctuated around 1500 μA cm^{-2} over the first 4 days of exposure. Shortly after that, its anodic activity began to drastically increase, reaching a peak of 5500 μA cm^{-2}, before falling to zero, as the Aspö groundwater in the exposure pool completely dried up. The total damage on the steel electrode, calculated using the CMEA technique, was 54.0×10^6 μm^3, which can be translated to an equivalent depth of 275 μm corrosion damage. The average corrosion rate on the steel electrode over this 6-day period of exposure was 17 mm $year^{-1}$, which was one order of magnitude higher than that following exposure to bentonite.

When evaluating the average cathodic current densities (Figure 4b), it can be seen that the cathodic activity was slightly higher at the corners and along the left side of the CMEA. This phenomenon is more pronounced when observing the cathodic activity at 5.4 days of exposure (Figure 4c), and is related to the formation of corrosion products, as shown by spectroscopic techniques (see results below).

3.4 | Spectroscopic investigation of the steel and copper surfaces analyzed

The extent and type of corrosion damage, as observed through microCT, can be seen in Figure 5. In both conditions of exposure, only the steel electrode (C3) was damaged as a result of corrosion. In the case of exposure to bentonite (Figure 5a), the total corroded volume was evaluated to be $9.4 \times 10^6\ \mu m^3$. Since the corrosion damage observed on the steel electrode was very uniform, the corroded volume could easily be transformed into corrosion damage, equaling 48 μm. In the case of exposure to groundwater (Figure 5b), the total corroded volume was evaluated to be $58.8 \times 10^6\ \mu m^3$. As previously, this resulted in total corrosion damage of approximately 300 μm. In both cases, these results are in-line with the CMEA results, where corrosion was only observed on the steel electrodes. The corrosion damage was calculated to be 47 and 275 μm following exposure to bentonite and groundwater, respectively.

After 13 days of exposure to the bentonite slurry, the 25 CMEA electrodes were inspected by SEM and Raman spectroscopy.

It can be seen from Figure 6 that the extent of the visible corrosion products on the steel electrode (C3) corresponds to the anodic currents measured and the corrosion damage observed with microCT. EDS analysis of the corrosion products on the surface of the steel electrode confirmed the presence of iron oxides (33 wt.% Fe and 29 wt.% O, on average). The corrosion products also contained lower amounts of elements as a result of the contact with bentonite (3.7 wt.% Si, 1.5 wt.% Al).

On the other hand, on the copper electrodes only cathodic currents were measured over the entire period of exposure. The electrodes along the outer edges of the CMEA (lines 1 and 5, columns A and E) were most cathodic, while lower cathodic currents were measured on the copper electrodes positioned around the central steel electrode (B2, B3, B4, C2, C4, D2, D3, and D4). A correlation was observed between the extent of the electrode deposits that were visible and the values of the cathodic currents measured; the higher the cathodic currents measured, the denser were the deposits at the surface (Figure 6). The deposit is a mixture of bentonite clay and corrosion products retained in the clay. EDS analysis of the copper electrodes, however, showed that

COLOR FIG

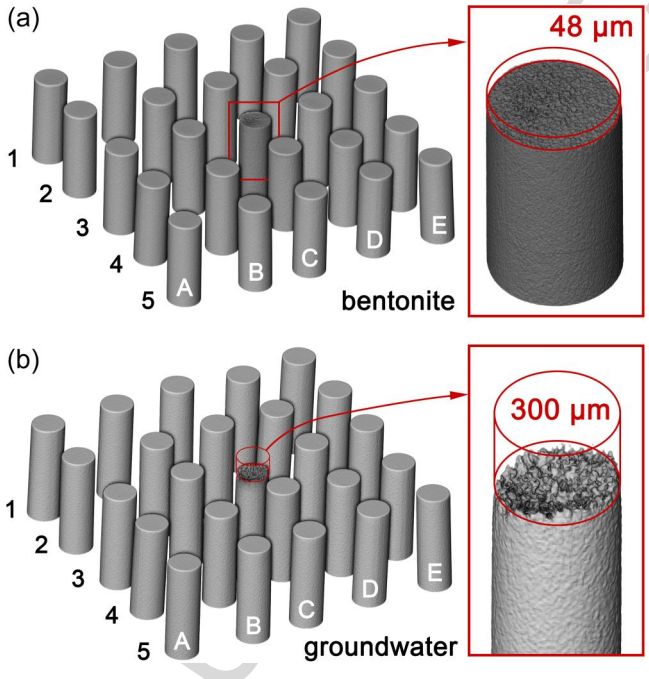

FIGURE 5 MicroCT of 24 copper and one carbon steel electrode (C3) following exposure to (a) bentonite slurry for 13 days and (b) Aspö groundwater for 6 days, both under standard ambient conditions.

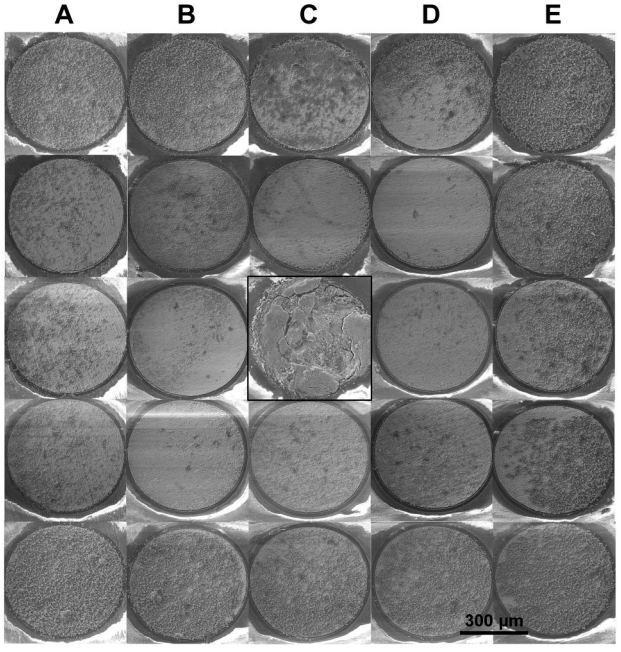

FIGURE 6 Scanning electron microscope images of the steel (C3) and copper (others) electrodes following 13 days exposure to bentonite slurry (170x magnification).

COLOR FIG

the surface was mainly covered with the remains of bentonite (due to presence of carbon and calcium). The copper surface without bentonite also contained copper oxides (containing around 10 wt.% Cu and 40 wt.% O), which was confirmed by Raman analysis, as shown below. The surfaces of all the electrodes also contained lower concentrations of chlorides from the ground water (up to 0.3 wt. %).

Several electrodes (the steel electrode [C3], two neighboring copper electrodes [D3 and C4], and a far distant electrode [E5]) were selected for a detailed spectroscopic study of the corrosion products formed over the surface, as presented in Figure 7.

In the bentonite slurry, thick corrosion products formed on the steel electrode (Figure 7a), consisting of lepidocrocite and goethite, as shown in the Raman spectra in Figure 7e.

Raman spectra measured on the steel electrode detected bands of lepidocrocite (γ-FeOOH) at 251, 376, 524, and 644 cm^{-1}. Lepidocrocite has been found to be unstable and porous,[23] and tends to dissolve and transform to other forms of oxide over time, thus offering weaker protection against corrosion. Raman spectra on the steel electrode also showed broad bands of goethite (α-FeOOH) at 301, 348, 478, and 556 cm^{-1}, as denoted by the arrows.

When comparing the copper electrodes D3, C4, and E5, differences were observed in the amount of bentonite deposited on the surface of the electrodes behaving net-cathodically. Small, rounded crystals were observed on the surface of the D3 copper electrode, while pitting was observed on C4, in addition to larger agglomerates of bentonite/corrosion products present at the surface (Figure C4). Raman spectra measured on both electrodes

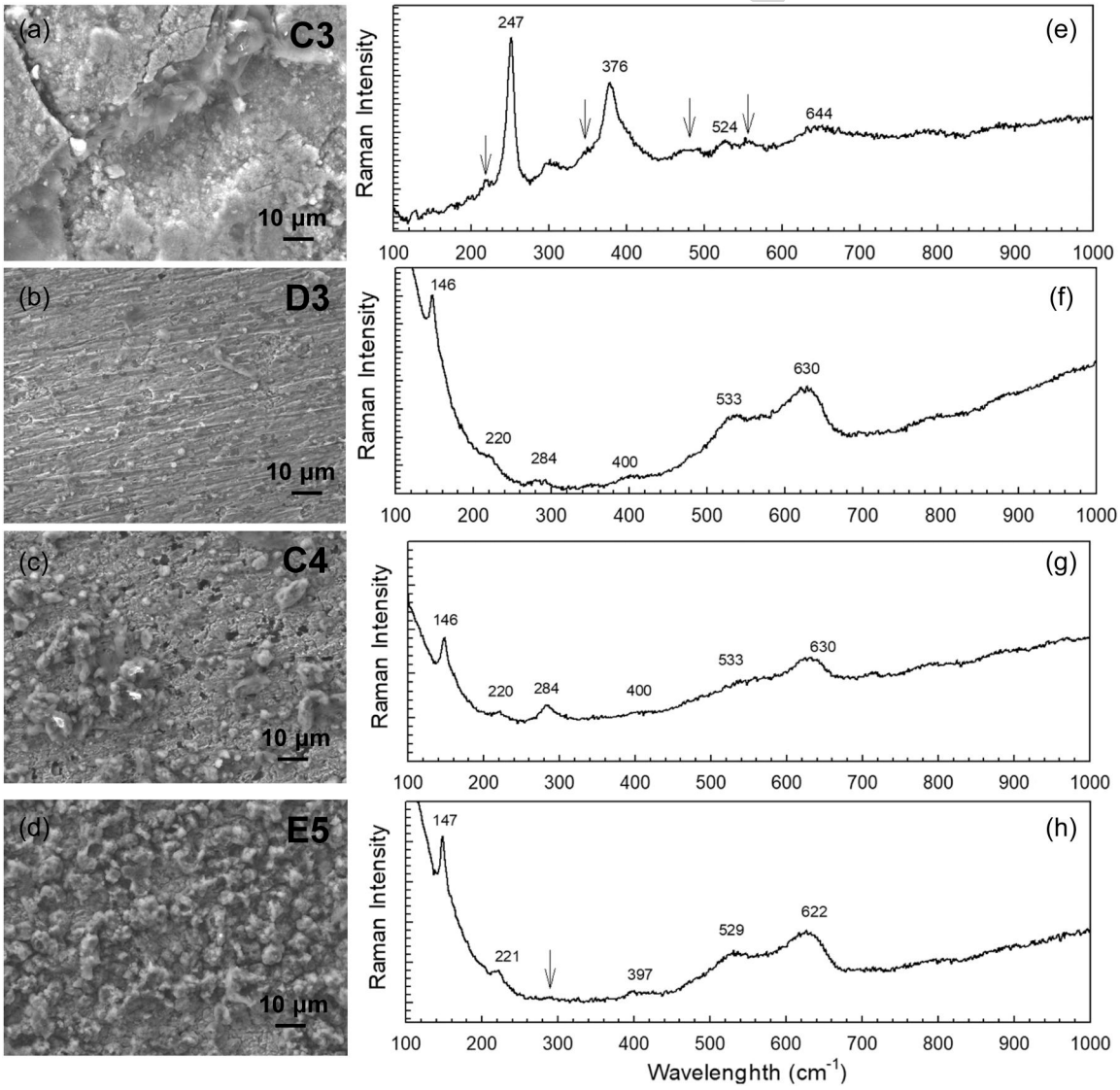

FIGURE 7 Images of the selected electrodes following 13 days exposure to bentonite slurry, inspected by scanning electron microscope at different magnifications (a–d), and Raman spectra (e–h) measured on the steel electrode, C3, and the copper electrodes D3, C4, and E5.

revealed the presence of Cu_2S, with bands identified at 146, 220, 400, 533, and 630 cm^{-1}, as well as a well-defined band characteristic of Cu_2S at 284 cm^{-1}.[16]

On the E5 electrode, however, which was heavily covered with corrosion products, deposits of cuprite were present in a higher percentage than Cu_2S. Raman spectra consisted of bands at 147, 221, 397, 529, and 622 cm^{-1}.[24]

4 | DISCUSSION

The intensive galvanic corrosion of the steel-copper coupling was monitored in simulated Aspö groundwater over the early days of exposure. The anodic current density of the CMEA steel electrode ranged from 1.0 to 1.5 mA cm^{-2} before the electrolyte drying out, which occurred around the 5th day. This value is in perfect agreement with the data obtained by Standish et al. [11] (Figure 3), where little difference was found between the galvanic current of Cu-steel couples of varying area ratios measured in aerated 0.1 M and 3 M NaCl solutions. In our study, an average corrosion rate of ~17 mm $year^{-1}$ was measured, while at the end of the exposure, an even higher rate of 63 mm $year^{-1}$ was observed, due to the accelerated corrosion reaction caused by the simulated groundwater, which contained chlorides, drying up.

The situation observed clearly demonstrates the importance of dissolved oxygen when considering the galvanic corrosion of steel in a steel-copper pair. The cathodic reaction on the copper surface predominantly relates to the reduction of oxygen. In the system with Aspö groundwater there was easy access to oxygen from air, and the anodic current density remained stable. The peak in corrosion activity at the end of the exposure was caused by an increase in conductivity and chloride concentration in the remaining electrolyte pool, which was very thin and thus enabled rapid diffusion of oxygen to the copper surface. A significant but uneven deposition of corrosion products on the copper electrodes (Figure 8) markedly reduced the contribution of the covered electrodes to the total cathodic current.

On the other hand, the steel electrode exhibited a significantly lower and decaying anodic current density in bentonite slurry compared to the steel electrode in the aqueous solution. The initial short peak, which exceeded 1.2 mA cm^{-2}, was, however, very high, and in good agreement with other studies.[11] In the first 5 days of exposure, the anodic current value was approximately 200 μA cm^{-2}, but it then decreased even further, resulting in an average value of 114 μA cm^{-2}, which is equal to a corrosion rate of approximately 1.3 mm $year^{-1}$. The steady reduction in the anodic current in this environment can most likely be attributed to the consumption of dissolved oxygen, which is reduced on the Cu surface and becomes the predominant cathodic reaction. Another potential mechanism could be the growth of corrosion products which, due to the bentonite overlay, are mostly immobile, and tend to concentrate close to the source of the anodic reaction.

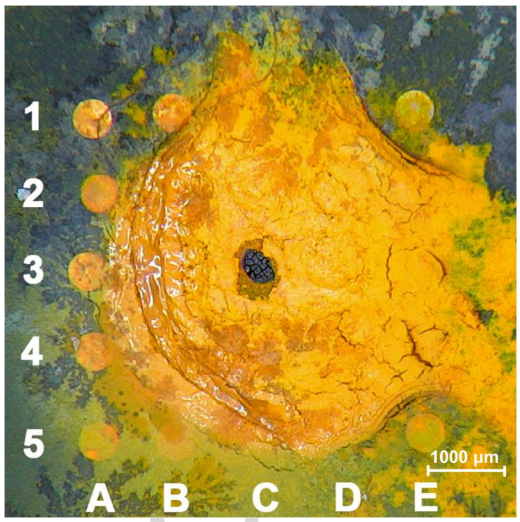

FIGURE 8 Corrosion products formed on the coupled multielectrode array (CMEA) electrodes following exposure to Aspö groundwater.

The question of the deficiency in dissolved oxygen requires further consideration. Careful examination of the cathodic currents in the bentonite system reveals that, until the 7th day, the four corner electrodes had the highest cathodic current density of all the copper electrodes, followed by the remaining electrodes positioned along the edges of the array. The next-closest neighbors of the central steel electrode (B4, D4, B2, and D2) exhibited current densities of roughly half those measured at the edges (excluding the corner electrodes). The nearest neighbors to the steel electrode (B3, D3, C4, and C2) exhibited the lowest cathodic current densities. The pattern described persists up to the 7th day and clearly demonstrates that dissolved oxygen is both scarce and quickly consumed by the copper electrodes, such that electrodes inside the array receive less oxygen and produce a lower cathodic current. No such pattern was observed in the Aspö groundwater system, where the A5 corner electrode acted as the most cathodic site. The cathodic current density was, however, far more uniformly distributed across the Cu electrodes than in the bentonite system. All these insights were possible thanks to the fact that the copper electrode was partitioned into several electrodes—a CMEA.

5 | CONCLUSIONS

The use of CMEA for measuring galvanic corrosion was demonstrated in the present study. By correctly arranging the coupled Cu and Fe electrodes, it was possible to monitor the localization of anodic processes as well as the distribution of cathodic processes.

Very high corrosion rates were measured in Fe coupled to Cu during the initial oxic phase. During the first part of exposure, the average corrosion rate in bentonite slurry soaked with simulated saline groundwater was approximately 1.3 mm per year. Even higher corrosion rates were measured in the aqueous solution (simulated saline groundwater), where values varied between 15 and 20 mm per year. It should be noted that just before drying out, the corrosion rate reached extreme values as high as 60 mm $year^{-1}$. The corrosion damage calculated from the anodic currents measured correlates well with results from micro CT measurements.

The steady reduction in corrosion rate observed in the bentonite slurry was most likely related to the consumption of dissolved oxygen, which is reduced on the Cu surface and is the predominant cathodic reaction. This was indicated by the uneven distribution of the cathodic current, which was largest in the copper electrodes positioned at the outer edges of the array.

Optical observation and Raman analysis on the corroded CMEA electrodes showed that the steel electrode was subjected to localized attack, with the presence of the corrosion product lepidocrocite, which is both porous and voluminous. On the copper electrodes exposed to bentonite slurry, both cuprite and Cu_2S were formed.

ACKNOWLEDGMENTS

This work was performed under Slovenian research agency (SRA) funding P2-0273 (Building structures and materials).

CONFLICT OF INTEREST STATEMENT

The authors declare no conflict of interest.

DATA AVAILABILITY STATEMENT

The data that support the findings of this study are available from the corresponding author upon reasonable request.

ORCID

Tadeja Kosec http://orcid.org/0000-0001-6790-1880
Nina Gartner http://orcid.org/0000-0002-3770-6555

REFERENCES

[1] F. King, L. Ahonen, C. Taxén, U. Vuorinen, L. Werme, *Copper Corrosion Under Expected Conditions in a Deep Geological Repository*, Technical report TR-01-23, Svensk Kärnbränslehantering AB, Stockholm **2001**.
[2] F. King, C. Lilja, K. Pedersen, P. Pitkananen, M. Vahanen, *An Update of the State of the Art Report on the Corrosion of Copper Under Expected Conditions in a Deep Geologic Repository*, Technical report TR-10-67, Svensk Kärnbränslehantering AB, Stockholm **2010**.
[3] N. Diomidis, L. H. Johnson, *JOM* **2014**, *66*, 461.
[4] B. Rosborg, J. Pan, *Electrochim. Acta* **2008**, *53*, 7556.
[5] M. Bojinov, I. Betova, C. Lilja, *Corros. Sci.* **2010**, *52*, 2917.
[6] J. M. Smith, J. C. Wren, M. Odziemkowski, D. W. Shoesmith, *J. Electrochem. Soc.* **2007**, *154*, C431.
[7] J. Smith, Z. Qin, F. King, L. Werme, D. W. Shoesmith, *Corrosion* **2007**, *63*, 135.
[8] J. Chen, Z. Qin, D. W. Shoesmith, *Electrochim. Acta* **2011**, *56*, 7854.
[9] T. Martino, J. Chen, Z. Qin, D. W. Shoesmith, *Corros. Eng. Sci. Technol.* **2017**, *52*, 61.
[10] T. Standish, J. Chen, R. Jacklin, P. Jakupi, S. Ramamurthy, D. Zagidulin, P. Keech, D. Shoesmith, *Electrochim. Acta* **2016**, *211*, 331.
[11] T. E. Standish, L. J. Braithwaite, D. W. Shoesmith, J. J. Noël, *J. Electrochem. Soc.* **2019**, *166*, C3448.
[12] T. E. Standish, D. Zagidulin, S. Ramamurthy, P. G. Keech, J. J. Noël, D. W. Shoesmith, *Corros. Eng. Sci. Technol.* **2017**, *52*, 65.
[13] L. Braithwaite, K. Albrechtas, D. Zagidulin, M. Behazin, D. Shoesmith, J. J. Noël, *J. Electrochem. Soc.* **2022**, *169*, 051502.
[14] B. Rosborg, T. Kosec, A. Kranjc, J. Pan, A. Legat, *Electrochim. Acta* **2011**, *56*, 7862.
[15] B. Rosborg, T. Kosec, A. Kranjc, V. Kuhar, A. Legat, *The Corrosion Rate of Pure Copper in a Bentonite Test Package Measured with Electric Resistance Sensors,* Technical report TR-13-15, Svensk Kärnbränslehantering AB, Stockholm **2012**.
[16] T. Kosec, Z. Qin, J. Chen, A. Legat, D. W. Shoesmith, *Corros. Sci.* **2015**, *90*, 248.
[17] T. Kosec, M. Hren, A. Legat, *Corros. Eng. Sci. Technol.* **2017**, *52*, 70.
[18] S. Matin, A. Tahmasebi, M. Momeni, M. Behazin, M. Davison, D. W. Shoesmith, J. J. Noël, *J. Electrochem. Soc.* **2022**, *169*, 061503.
[19] D. S. Hall, M. Behazin, W. Jeffrey Binns, P. G. Keech, *Prog. Mater. Sci.* **2021**, *118*, 100766.
[20] B. Reddy, C. Padovani, A. P. Rance, N. R. Smart, A. Cook, H. M. Haynes, A. E. Milodowski, L. P. Field, S. J. Kemp, A. Martin, N. Diomidis, *Mater. Corros.* **2020**, *72*, 361.
[21] A. Legat, *Electrochim. Acta* **2007**, *52*, 7590.
[22] A. Česen, T. Kosec, A. Legat, *Corros. Sci.* **2013**, *75*, 47.
[23] J. K. Singh, D. D. N. Singh, *Corros. Sci.* **2012**, *56*, 129.
[24] R. L. Frost, *Spectrochim. Acta, Part A* **2003**, *59*, 1195.

How to cite this article: T. Kosec, M. Hren, K. Prijatelj, B. Zajec, N. Gartner, A. Legat, *Mater. Corros.* **2023**, 1–9.
https://doi.org/10.1002/maco.202213689